

ARTICLE OPEN



Experimental investigation of porous carbon for cooling and desalination applications

Ahmed S. Alsaman¹, M. Salem Ahmed¹, E. M. M. Ibrahim², Ehab S. Ali³, A. M. Farid³ and Ahmed A. Askalany¹✉

Adsorption cooling and desalination (ACD) system presents a solution for water, energy, and environmental dilemma. This study expresses an enhancement of adsorption system performance in terms of cooling and desalination effects by improving an activated carbon Maxsorb III (Max) as an adsorbent. Max has been initially treated with HCl. Then, it has been activated by impregnating it in salt hydrates ((NH₄)₂CO₃). Characterization methods, including XRD, N₂ and water adsorption isotherm, and water adsorption kinetics have been conducted for raw Max, treated Max, and activated Max with (NH₄)₂CO₃. The experimental values have been fitted with the Dubinin & Astakhov equilibrium model for isotherm and the model of linear driving force for kinetics. These fitted parameters have been utilized in a previously validated model to estimate adsorption cooling-desalination system performance with and without heat recovery. Max/(NH₄)₂CO₃ achieves a water uptake of 0.53 kg_{H₂O}.kg⁻¹. Max/(NH₄)₂CO₃ produces 13.2 m³.ton⁻¹ of freshwater per day with a specific cooling power of 373 W.kg⁻¹ and 0.63 COP. Also, the freshwater reaches 22.5 m³.ton⁻¹ of Max/(NH₄)₂CO₃ per day with condenser-evaporator heat recovery. These results indicate the potential of utilizing the Max material in dual cooling and desalination applications to achieve double what silica gel can offer.

npj Clean Water (2023)6:4; <https://doi.org/10.1038/s41545-022-00211-z>

INTRODUCTION

Energy and water desalination became one of the most important research fields that attract scientists to find a sustainable solution for energy and water shortage. Such a solution mainly depends on utilizing renewable energy sources like waste energy from electrical energy plants or nuclear plants etc, or solar energy. The conventional cooling and desalination methods consume relatively high energy and mainly depend on fossil fuels and electricity^{1–3}. Cooling and desalination applications based on adsorption systems become a solution for these problems. They could be powered efficiently by low-temperature heat sources or waste energy^{4–6}. Adsorption system has advantages such as it could generate double effect cooling and desalination. It has no moving parts. Desalinated water produced by the adsorption system has very good water quality, less than 10 ppm^{7,8}.

An adsorption system usually consists of 2 or more beds, a condenser, and an evaporator. The adsorption systems in some studies also contain more than one evaporator^{5,9}, and they can work as a single or two-stage^{9–11}. In adsorption cooling and desalination (ACD) systems, the heat generated during adsorption process (heat of adsorption (H_{st})) and condensation heat are removed by passing the cooling water through the heat exchangers. The required heat for evaporation is added from an external cooling load. In the case of desalination only (adsorption desalination with heat recovery (AD-HR)), the heat of condensation required for condensation is exploited as heat for evaporation by making condenser/evaporator heat exchange. The system can be powered by thermal energy heat sources such as solar energy, biomass, geothermal energy, and waste heat. Figure 1 shows a schematic of a 2-bed adsorption system. The green lines are the heat transfer lines by water flow from the evaporator to the condenser and back.

The research directions for ACD represent how to enhance the coefficient of performance (COP) and increase the cooling effect

and specific water production per ton of adsorbent material per day (SDWP). This can be achieved by improving the system design to increase the overall heat transfer coefficient. There are some theoretical studies on the hybridization of the AD system with thermal desalination plants^{4,5,12,13}. Also, the researchers improve these systems' performance by finding new adsorbent materials with high adsorption capacity (Ad-C)^{8,14–20} or improving available adsorbents^{19–29}. Ng et al.³⁰ confirmed that the SDWP for the adsorption systems could be optimized linearly with both evaporator and heat source temperatures. Chakraborty et al.³¹ developed the surface thermodynamic properties of silica gel (SG) to optimize ACD systems' performance. Mitra et al.³² presented a two-stage ACD system using SG as an adsorbent and air-cooled. The results showed that, with air-cooled, the two-stage ACD system performance was significantly lower than single-stage systems with water-cooled. But, the two-stage ACD system can be operated at 53 °C air temperature with a 16 °C chilled water inlet, which makes it suitable for climatic conditions in hot regions. Thu et al.³³ investigated a numerically 4-bed AD-HR system. The results observed that the AD-HR cycle could be operated at 50 °C heat source temperature. The results also illustrated that the 4-bed adsorption system with heat recovery could produce about 60% more fresh water than the conventional adsorption system (2-bed without heat recovery).

Many researchers studied the effect of alkalization and acidification with different concentrations on different adsorbents such as clay^{22,34–38}, zeolite^{23,34}, vermiculite³⁴, SG³⁹, and metal-organic frameworks (MOF)⁴⁰. The acid/alkaline activation is the most common chemical enhancement for adsorbents by removing the octahedral cations. The adsorbents can be activated using an acid solution; usually, HCl, to increase the S_{BET} (surface area by Brunauer-Emmett-Teller) and V_{por} (pore volume)⁴¹. Increasing the S_{BET} of the material leads to an increase in the Ad-C^{42,43}. For example on acid and alkaline activation, Jozefaciuk et al.³⁴ studied

¹Mechanical Department, Faculty of Technology and Education, Sohag University, Sohag 82524, Egypt. ²Physics Department, Faculty of Science, Sohag University, Sohag 82524, Egypt. ³Mechanical Engineering Department, Tabbin Institute for Metallurgical Studies, Cairo 11912, Egypt. ✉email: ahmed_askalany3@yahoo.com

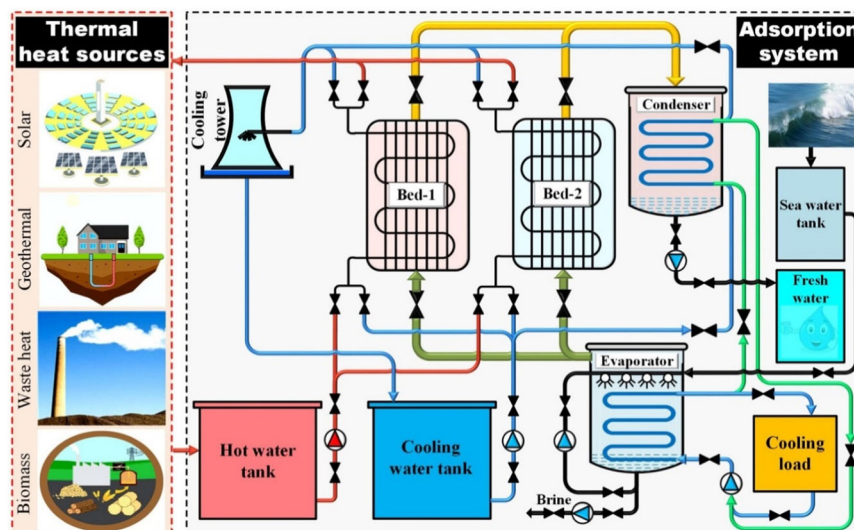


Fig. 1 Adsorption system for cooling and desalination applications with different thermal heat sources. The system consists of 2 beds, a condenser, and an evaporator, in addition to the complementary parts such as the cooling tower, cooling, heating and desalinated water tanks, water flow pumps and valves. The green lines are the heat transfer lines by water flow from the evaporator to the condenser and back.

the effect of alkalization and acidification on bentonite, biotite, illite, kaolin, vermiculite, and zeolite by adding sodium hydroxide or hydrochloric acid. In alkali and acid activation, surface areas and adsorption capacities increase with reagent concentrations. Askalany et al.²² modified bentonite material by acid activation using HCl for water adsorption applications. The S_{BET} and V_{por} increased by about 800% and 1340%, respectively, increasing the water Ad-C by about 200%. The results also illustrated that the COP and specific cooling power (SCP) had 0.55 and 150 W.kg⁻¹ values, respectively. Ali et al.³⁷ studied the adsorption properties of montmorillonite clay activated by HCl. The activation process was performed by mixing the clay material with 0.5–2 M HCl. The activation increased the S_{BET} and V_{por} values by about 180% and 460%, respectively, leading to increased water Ad-C by about 180%. The COP, SCP, and SDWP had 0.46, 110.4 W.kg⁻¹, and 4.17 m³.ton⁻¹, respectively.

HCl and plasma were used for zeolite activation²³, and the water Ad-C was 0.165 kg.kg⁻¹ by a percent enhancement of 11.54. Mota et al.³⁹ enhanced the water Ad-C of SG adsorbent using acid activation. Noteworthy, the highest water vapor Ad-C was observed for the sample treated without adding an acidic catalyst. Teo et al.⁴⁰ optimized MOFs adsorbent materials by synthesizing (aluminum fumarate) MOFs with formic acid. The results showed a maximum performance for the sample activated using the formic acid 10 mL concentration, where the S_{BET} and V_{por} were 836 m².g⁻¹ and 0.44 cm³.g⁻¹.

Many researchers studied the effect of composite different carbon types with different concentrations of salt hydrates to increase Ad-C. For example, Gordeeva et al.⁴⁴ studied water Ad-C of expanded graphite/LiBr (SWS-2EG) carbon and Sibunit/LiBr (SWS-2C) composites. Both the composites achieved water vapor Ad-C of 1.1 kg.kg⁻¹ at 0.7 P/P_s. Tso et al.⁴⁵ studied the AC/SG/CaCl₂ composite adsorption properties. The Ad-C achieved 0.23 kg.kg⁻¹ at 0.9 kPa and 0.805 kg.kg⁻¹ at atmospheric pressure. The SCP and COP improved by 372% and 92%, respectively. Huang et al.⁴⁶ prepared two composites of AC (AC1/Na₂SiO₃ and AC2/Na₂SiO₃). The AC1/Na₂SiO₃ and AC2/Na₂SiO₃ composites exhibited about 5.9 and 2.6 times higher water Ad-C than pure activated carbon. Casey et al.⁴⁷ prepared different composites (SIM-4_a to _e) composites with different salt hydrates as thermal storage materials. The Ad-C was 0.49 kg.kg⁻¹ of SIM-4_a at P/P_s > 0.6. Yu et al.⁴⁸ synthesized AC/MgCl₂/Ce as a new composite material. The water was about 1.05 kg.kg⁻¹. Grekova et al.^{49,50} studied the

adsorption characteristics of multi-wall carbon nanotube (MWCNT) with CaCl₂ and LiCl. The Ad-C achieved 1 kg.kg⁻¹ of composites. The water Ad-C for LiCl/MWCNT/PVA achieved 0.6 kg.kg⁻¹ at 35 °C⁵¹. Alsaman et al.¹⁹ summarized enhancement conditions and properties of the adsorbent materials. This paper studied enhancing the performance of ACD systems by improving the Max adsorbent material by activation method using an ammonium carbonate ((NH₄)₂CO₃).

RESULTS AND DISCUSSION

Structure and porosity analysis

Morphological analysis of the Max by scanning electron microscopic (SEM) for 4000 times is shown in Fig. 2a–c. The morphological analysis indicates that the (NH₄)₂CO₃ would remarkably increase the surface microstructure of Max and vice versa with HCl. X-ray diffraction (XRD) patterns analysis of Max samples is shown in Fig. 2d. From the figure, raw and modified Max samples have graphite (Gr) hump at 42.5°. No change can be observed by treatment and activation processes. This means no change in the crystallization of the material due to its strong structure. It is also clear from the figure that the modified Max has no aging effect due to no change in the material's structure. Figure 2e displays nitrogen (N₂) adsorption-desorption isotherms of raw Max, Max/HCl, and Max/(NH₄)₂CO₃ samples. The figure explains the same curve behavior of Max samples nitrogen adsorption-desorption. The Max/HCl has the lowest N₂ uptake, possibly caused by the low porosity. The highest N₂ is adsorbed by Max/(NH₄)₂CO₃, then raw Max. The porosity properties of raw and modified Max are illustrated in Table 1. Figure 2 and Table 1 illustrate that Max N₂ isotherms are closest to the I-Type, and the Max has microporous pore sizes (< 2 nm) according to IUPAC classification⁵².

Water equilibrium analysis

Water Ad-C values of the raw, acid-treated, and activated Max adsorbents are plotted as a function of P/P_s in Fig. 3a–d. As shown in Fig. 3a, the highest water Ad-C corresponds to Max/(NH₄)₂CO₃ (0.52 kg.kg⁻¹) at 25 °C and 0.9 P/P_s, followed by Max/HCl (0.42 kg.kg⁻¹). Figure 3b–d illustrates the water vapor Ad-C onto raw and modified Max with their D-A model fittings at different adsorption temperatures (Ad-T). The H_{st} generated during the

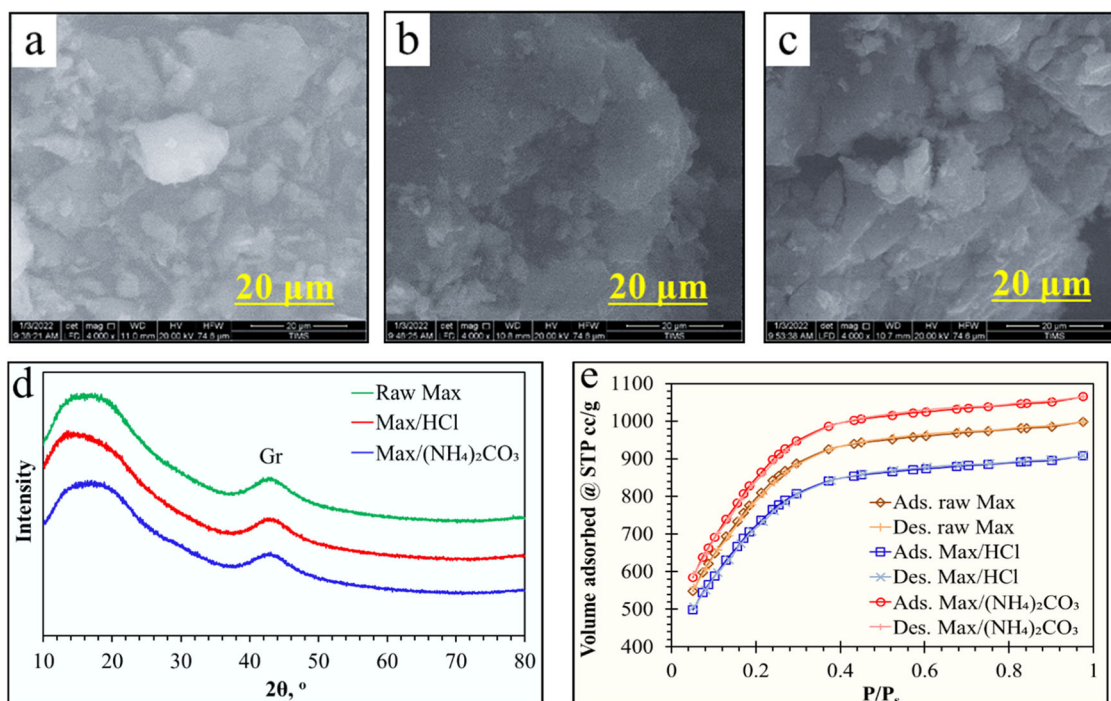


Fig. 2 Materials structure and porosity analysis. **a** SEM image of raw Max, **b** SEM image of Max/HCl, **c** SEM image of Max/(NH₄)₂CO₃, **d** XRD of Max samples, and **e** N₂ adsorption-desorption isotherms of raw and modified Max. No change can be observed Max structure. Max N₂ isotherms are closest to the I-Type, and the Max has microporous pore sizes.

Table 1. Porosity characteristics, D-A, and LDF fitted parameters of Max samples.

Characterization	Item	Unit	Raw Max	Max/HCl	Max/(NH ₄) ₂ CO ₃
Porosity	S _{BET}	m ² .g ⁻¹	2873.61	2612.37	3065.18
	V _{0.99}	cm ³ .g ⁻¹	1.55	1.41	1.65
	Pore size	nm	1.078	1.078	1.078
	R _p	nm	0.47454	0.52199	0.44488
Isotherm (D-A fitted)	C _o	kg.kg ⁻¹	0.175	0.350	0.530
	E	kJ.kg ⁻¹	3571.78	4082.73	4116.73
	n	–	1.68	1.62	1.70
	Average H _{st}	kJ.kg ⁻¹	2799.13	2833.88	2869.93
Kinetics (LDF fitted)	E _a	kJ.mol ⁻¹	3059.3	4157	4013.3
	D ₅₀	m ² .s ⁻¹	2.88192E-23	1.49032E-23	2.31511E-23
	F _o	–	37	35	46

adsorption process is estimated for raw and modified Max utilizing D-A parameters fitting with experimental results. The D-A fitted parameters and H_{st} are listed in Table 1.

Figure 3e–h demonstrates the kinetics of samples. Initially, all Max samples display around equivalent values, as shown in Fig. 3e. Max/(NH₄)₂CO₃ displays the highest kinetics uptake. The Max/HCl kinetics uptake performs less than Max/(NH₄)₂CO₃. The raw Max achieves the lowest kinetics uptake, which expresses the successful activation for Max samples. Figure 3f–h displays the Max samples fitted LDF for the experimental kinetics with outstanding agreement at several Ad-T. Table 1 displays the fitted values of Max samples kinetics uptake.

Figure 4a displays water vapor Ad-C against Polanyi adsorption potential ($-RT \ln(P/P_s)$) to realize how Max samples perform better in cooling and desalination applications. Evaporation pressures (P_{evap}) are selected to be 1 kPa and 2.25 kPa for cooling and desalination, respectively. The condensation pressure (P_{cond})

is selected to be 3.2 kPa. The Ad-T is 25 °C, and De-T is 85 °C, respectively. The available difference in water Ad-C at the adsorption and desorption pressures (ΔC) is the most significant characteristic of cooling and desalination effects. For dual-purpose (cooling & desalination) (at P_{evap} = 1 kPa), Max/(NH₄)₂CO₃ has the highest ΔC (0.27 kg.kg⁻¹), then Max/HCl with (0.17 kg.kg⁻¹) and lastly raw Max with (0.07 kg.kg⁻¹). For desalination only (at P_{evap} = 2.25 kPa), Max/(NH₄)₂CO₃ has the highest ΔC (0.47 kg.kg⁻¹), then Max/HCl (0.3 kg.kg⁻¹) and lastly raw Max with (0.15 kg.kg⁻¹).

Figure 4b–d indicates a P-T-C (Pressure-Temperature-Capacity of water vapor) plot of the raw and modified Max-based ACD and AD-HR cycles. The figure shows that the Max/(NH₄)₂CO₃ has about 400% water vapor Ad-C than raw Max during the ACD cycle. For the AD-HR cycle, the Max/(NH₄)₂CO₃ have about 300% water vapor Ad-C than raw Max. The figure also displays that the AD-HR cycles have double the water vapor Ad-C of the ACD cycle.

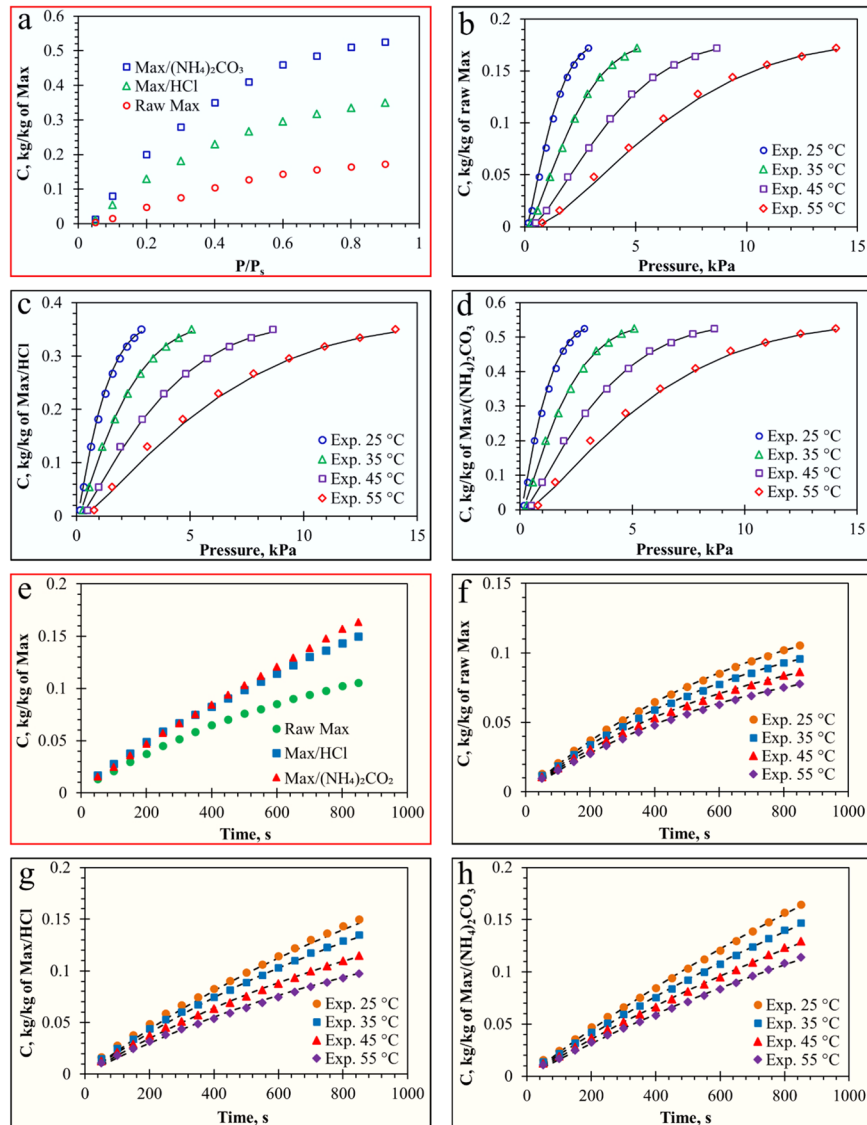


Fig. 3 Water equilibrium analysis for Max samples. **a** Max samples Ad-Iso at 25 °C, **b** raw Max Ad-Iso, **c** Max/HCl Ad-Iso, **d** Max/(NH₄)₂CO₃ Ad-Iso, **e** Max samples Ad-Kin at $P/P_s = 0.9$ and Ad-T = 25 °C, **f** raw Max Ad-Kin, **g** Max/HCl Ad-Kin, and **h** Max/(NH₄)₂CO₃ Ad-Kin. Max/(NH₄)₂CO₃ displays the highest water Ad-C for isotherms and kinetics uptake.

Adsorption system performance

Figure 5a, c, e shows the effect of t_{cycle} on the SCP, COP, and SDWP for raw and modified Max-based ACD cycle at 85 °C desorption temperature (De-T) and 25 °C Ad-T. The figure illustrates that the Max/(NH₄)₂CO₃ achieved higher performance with SCP, COP, and SDWP of about 373 W.kg⁻¹, 0.63, and 13.2 m³.ton⁻¹ per day at 350 s half t_{cycle} . The Max/HCl-based ACD cycle gives about 200 W.kg⁻¹ SCP, 0.53 COP, and 7 m³.ton⁻¹ per day SDWP. Finally, the raw Max achieves 147 W.kg⁻¹ SCP, 0.5 COP, and 5.2 m³.ton⁻¹ per day SDWP. Figure 5b, d, f shows the ACD cycle's performance with desorption temperature for raw and modified Max at 25 °C Ad-T and 350 s half t_{cycle} . The Max/(NH₄)₂CO₃ shows higher performance. The figure also illustrates an increase in the SCP and SDWP with increasing De-T. The optimum COP is recorded at 75 and 85 °C.

The system performance is investigated for raw and modified Max based-AD-HR cycle. Figure 6a, c shows the effect of t_{cycle} on SDWP and GOR at 85 °C De-T and 25 °C Ad-T. The Max/(NH₄)₂CO₃ illustrates higher performance with optimum SDWP and GOR values of about 22.5 m³.ton⁻¹ per day and 0.7 GOR at half $t_{\text{cycle}} = 350$ s. Figure 6b, d shows the SDWP and GOR with De-T

at 25 °C Ad-T and half 350 s. The Max/(NH₄)₂CO₃ shows higher performance. The figure also illustrates that the SDWP increases with increasing De-T. The opposite is for COP, where the COP decreases slightly with increasing De-T.

Figure 7a–c compares the TBed (bed temperature) and C (adsorption water uptake) for ACD and AD-HR cycles utilizing raw and modified Max at operating conditions of 25 °C T_{ch} and Ad-T and a thermal heat source with 85 °C. From the figure, the highest water Ad-C occurs with the AD-HR cycle due to working the adsorption cycle at an upper evaporation pressure than the ACD cycle. The figure shows that the ACD and AD-HR cycles can be operated efficiently with a thermal heat source of less than 100 °C regeneration temperature. Figure 8 compares the present study (raw and modified Max) with previous studies (based on SG)^{11,15,53–57} for SCP, COP, and SDWP based-dual effect ACD cycle at 85 °C De-T. The figure expresses the ability of Max/(NH₄)₂CO₃ to produce around double what SG could produce for dual cooling and desalination applications.

This study experimentally expresses the characterization of raw Max, Max/HCl, and Max/(NH₄)₂CO₃ to enhance the adsorption system performance. XRD, N₂ adsorption, characterized Max

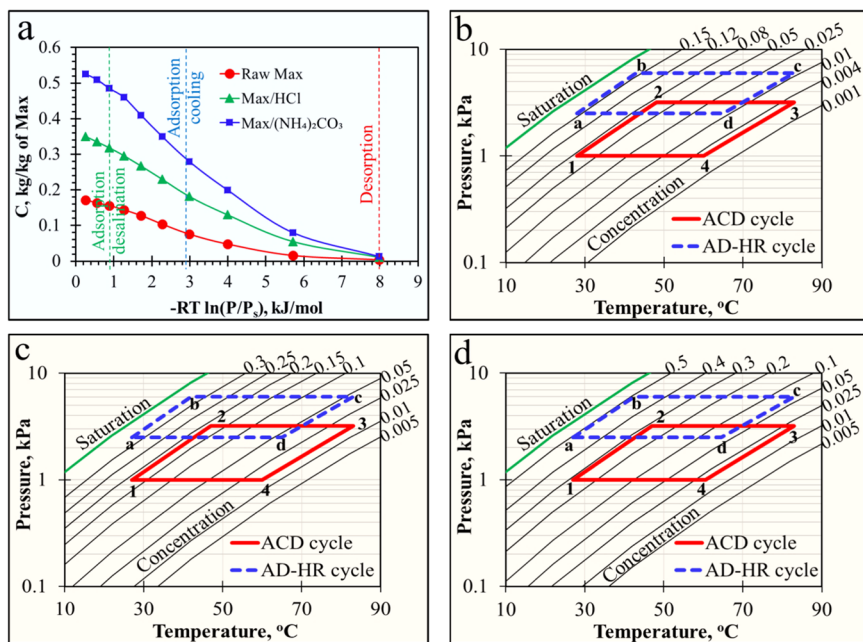


Fig. 4 Adsorption characteristic curves of water vapor on Max samples. **a** Gibbs energy change ($-RT \ln(P/P_s)$) relationship, **b** raw Max P-T-C diagram, **c** Max/HCl P-T-C diagram, and **d** Max/(NH₄)₂CO₃ P-T-C diagram. The AD-HR cycles have double the water vapor Ad-C of the ACD cycle.

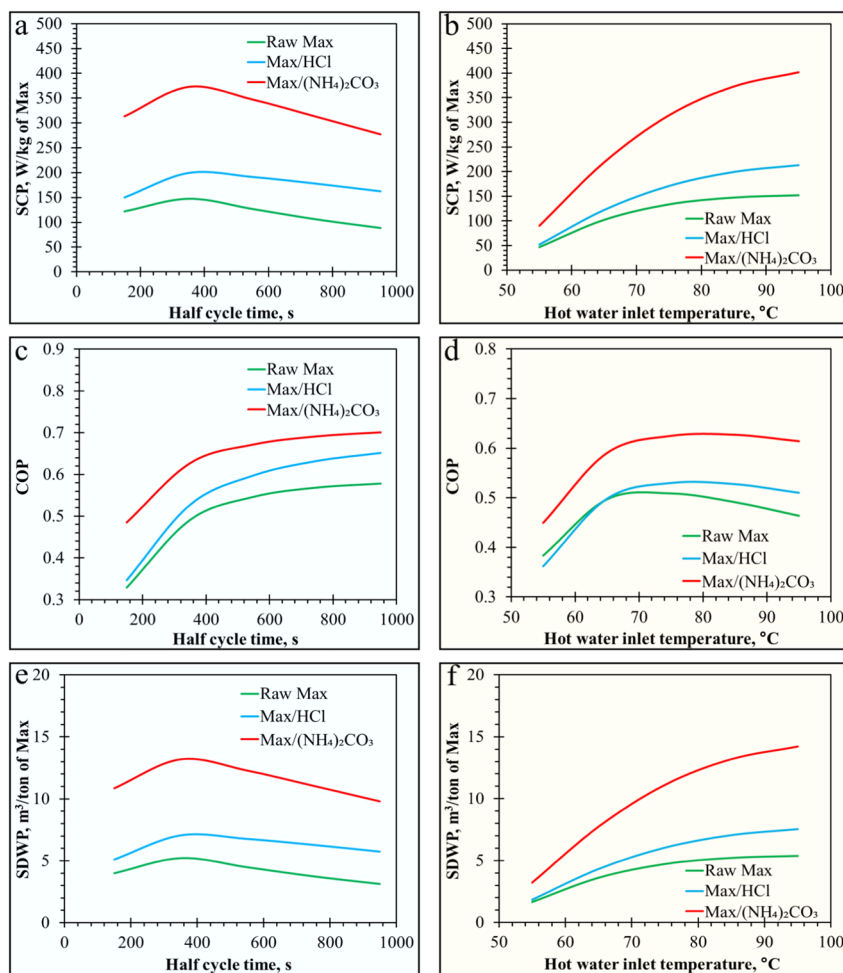


Fig. 5 ACD cycle performance. **a** SCP with a different half t_{cycle} , **b** SCP with a different De-T, **c** COP with a different half t_{cycle} , **d** COP with a different De-T, **e** SDWP with a different half t_{cycle} , and **f** SDWP with a different De-T. The optimum SCP and SDWP of raw and modified Max were recorded at 350 s half t_{cycle} . Both SCP and SDWP rise as the De-T increases.

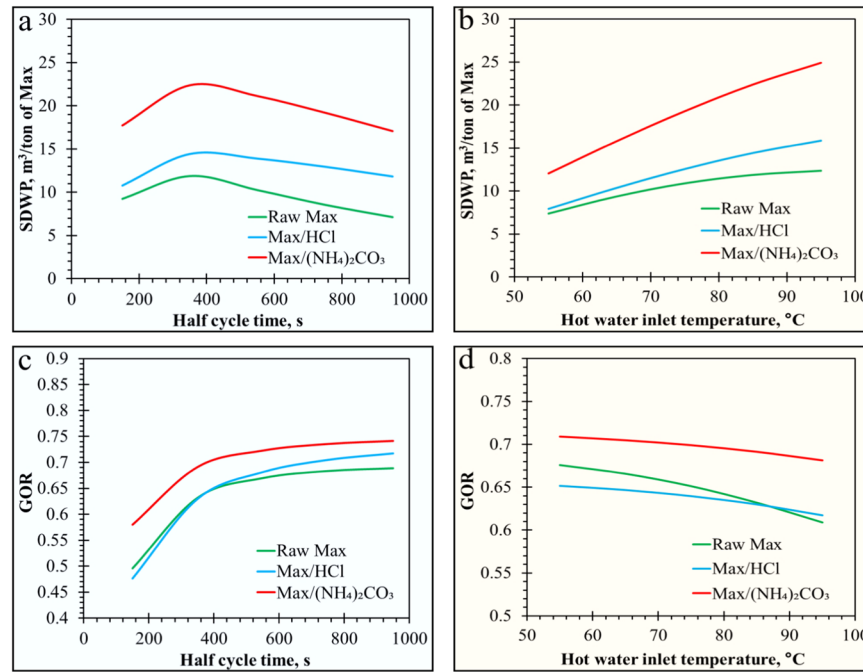


Fig. 6 AD-HR cycle performance. **a** SDWP with different half t_{cycl} , **b** SDWP with different De-T, **c** GOR with different half t_{cycl} , **d** GOR with different De-T. The optimum SDWP of raw and modified Max was recorded at 350 s half t_{cycle} . The SDWP rise as the De-T increases with a slight decrease in GOR.

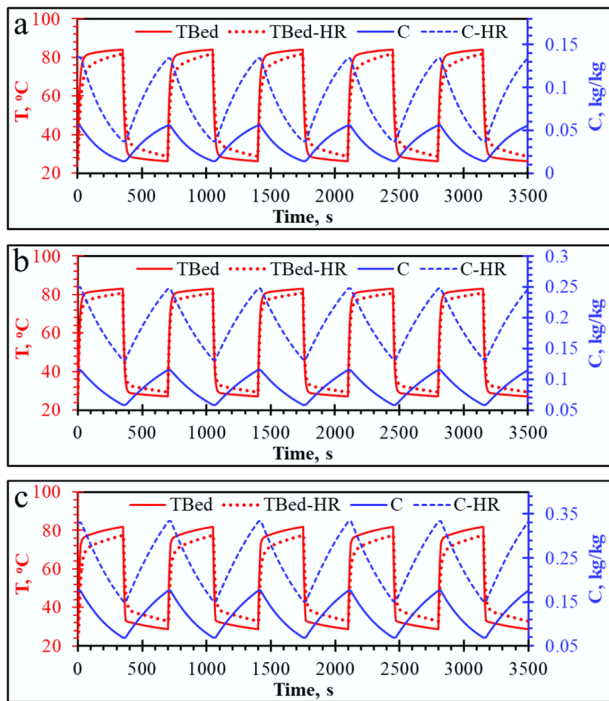


Fig. 7 Comparison of the TBed and the change in C during adsorption cycle for ACD and AD-HR cycles utilizing. **a** Raw Max, **b** Max/HCl, and **c** Max/(NH₄)₂CO₃ adsorbents. Due to working the adsorption cycle at an upper evaporation pressure than the ACD cycle, the highest water Ad-C occurs with the AD-HR cycle.

samples. The samples are tested for adsorption isotherm (Ad-Iso). Max/(NH₄)₂CO₃ achieved high Ad-C with 0.52 kg_{H₂O}.kg⁻¹ at 90% P/P_s. The samples are tested for adsorption kinetics (Ad-Kin). Isotherm and kinetics fitted values were utilized in the validated ACD lumped model to estimate adsorption system

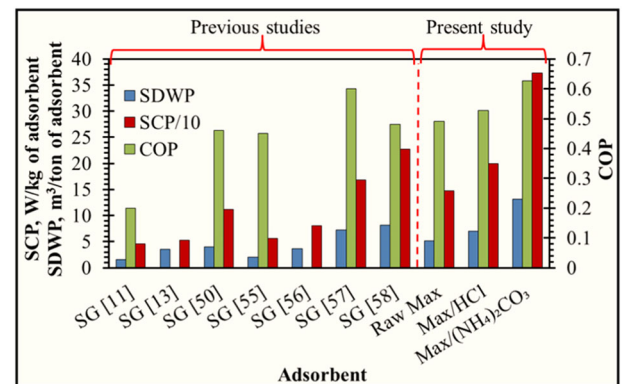


Fig. 8 Comparing the raw and modified Max-based ACD cycle performance with previous studies^{11,15,53–57} at 85°C De-T. The Max/(NH₄)₂CO₃ performance is about double SG performance for dual cooling and desalination applications.

performance. Max/(NH₄)₂CO₃ achieved the highest performance with SCP 373 W.kg⁻¹, COP 0.63, and SDWP 13.2 m³.ton⁻¹ for the ACD cycle. The AD-HR cycle obtains high water production. The highest SDWP is 22.5 m³.ton⁻¹ per day using Max/(NH₄)₂CO₃. This result expresses the ability of Max/(NH₄)₂CO₃ to produce around double what silica gel could produce for dual cooling and desalination applications. There is still a need to improve the Ad-C of the adsorbent materials, which calls for future work on this in several ways, such as activation and composition utilizing different salt hydrates.

METHODS

Materials

Maxsorb is a commercial production of high surface area activated carbon AX21-Type obtained from Japan (Kansai Coke & Chemicals Co. Ltd.). Max is manufactured by molten KOH with activating

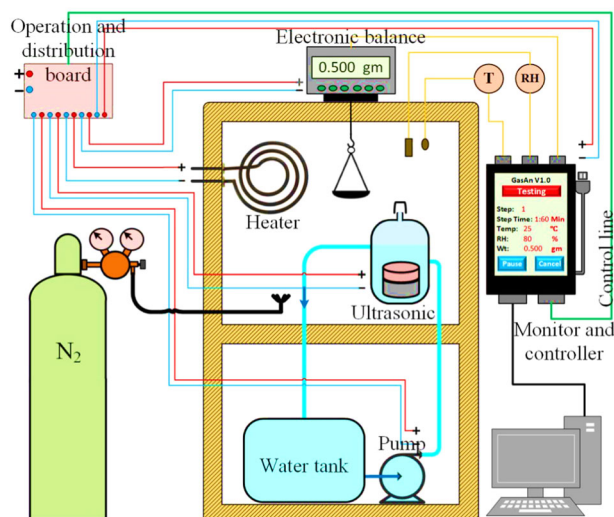


Fig. 9 Schematic of water adsorption apparatus. It was used to measure the adsorption isotherms and kinetics of the Max samples.

petroleum coke in a process patented by Standard Oil Company⁵⁸. It has been chosen due to its high porosity, large surface area, and low density. To prepare the modified Max, 2 M HCl is treated with 10 g of Max as a pretreatment for 12 h at RT with stirring. The mixture is leached, washed, and dried at 150 °C for 12 h. After acid treatment, 2.1 g of dried Max has been impregnated with 30 wt.% (NH₄)₂CO₃ dissolved in distilled water at RT for 24 h. The mixture is filtered and then dried at 150 °C for 12 h in an oven until it reaches a constant weight (initial weight due to (NH₄)₂CO₃ evaporation upon reaching 58 °C).

Characterization

Images of Max samples were acquired by scanning electron microscopic analysis to observe the microstructure and morphology of Max samples. Different investigation methods have been considered, including XRD, N₂ adsorption isotherm, and water vapor equilibrium, to characterize raw, treated, and activated Max. The raw and modified Max structure are characterized by XRD under ambient conditions by Bruker Axs-D & Advance diffractometer with Cu K α radiation ($\lambda = 1.5406 \text{ \AA}$) over the scan angle 2θ (10–80°). The N₂ adsorption-desorption isotherm method is utilized to estimate the porosity (S_{BET} and total pore volume ($V_{0.99}$)) of Max samples at $-196 \text{ }^\circ\text{C}$ by a Quantachrome TouchWin™ instrument. Raw and modified Max are degassed at 150 °C for 10 h before measuring. The S_{BET} and $V_{0.99}$ are found at the P/P_s of 0.3 and about 0.99, respectively.

Water vapor adsorption isotherm (Ad-Iso) and adsorption kinetics (Ad-Kin) of raw Max, Max/HCl, and Max/(NH₄)₂CO₃ are expressed by a direct weighing technique via a water vapor adsorption analyzer (Tabbin Institute for Metallurgical Studies, Egypt). Figure 9 displays the utilized apparatus, which involves 1) weighing sample chamber through adsorption with electronic balance; 2) Ultrasonic to create water vapor which is used to increase humidity; 3) an electric heater to control the adsorption runs at different temperatures; 4) humidity sensor; 5) a temperature sensor; 6) system controller to procedure all operation and saving data. The sample chamber is linked to a nitrogen cylinder for the degassing process. The humidity sensor is very near to the tested sample to ensure that it measures the tested sample's humidity. In addition, the tested chamber is 25 × 25 × 25 cm and has two vapor distributors. A detailed description of the water vapor adsorption analyzer can be found in Ref. ⁵⁹. For procedure experiments, 0.4 g of the Max has been located on the electronic balance. Then the Max sample is

evacuated under 100 °C with passing nitrogen (99% purity) for 10 h. The sample is cooled to the adsorption temperature (Ad-T) with passing nitrogen (99% purity).

For Ad-Iso, the system control is turned to Ad-Iso mode in which humidity (RH) is set to be varied from 5 to 90% through 18 steps. In each step, the controller fixes RH with $\pm 1\%$ of preset RH and records (temperature, RH, and sample weight). The Ad-Iso step ended when the stability of balance reading occurred within 0.002 g for 15 min. Then, the controller shifts the Ultrasonic to the following RH step. For Ad-Kin, the system control is turned to Ad-Kin mode, in which RH is set to be 90% through one step. The controller rises RH from 0 to 90% and then fixes RH with $\pm 1\%$ and temperature $\pm 0.5 \text{ }^\circ\text{C}$ and records (temperature, RH, and sample weight) with time from 0 to 850 s. Then, the controller repeats this procedure for 25–55 °C Ad-T.

AD SYSTEM MATHEMATICAL MODEL

A mathematical model is used to estimate adsorption systems' performance indicators, represented in SCP, COP, and SDWP for the ACD system and SDWP and gained output ratio (GOR) for the AD-HR system for higher water production. The model includes water equilibrium equations D-A (Dubinin & Astakhov) and LDF (linear driving force) for adsorption isotherm and kinetics, respectively) and each system component's mass and energy balance equations. The adsorption system considered in the present study has two beds, an evaporator, and a condenser. The used model in the present study is validated with experimental work⁵⁵ and published in many references^{20,21,29,37,60}. The main parameters and conditions used in the theoretical model are stated in Ghazy et al.⁶¹.

Water equilibrium

An experimental investigation of adsorption for suggested materials has been done utilizing a water vapor sorption analyzer. The raw and modified Max experimental values have been fitted with the D-A model by Eq. (1)⁵⁵.

$$C = C_o \exp \left\{ - \left(\frac{RT}{E} \ln \left(\frac{P_s}{P} \right) \right)^n \right\} \quad (1)$$

H_{st} can be expressed by Eq. (2)⁵⁵;

$$H_{st} = h_{fg} + E \left[\ln \left(\frac{C_o}{C} \right)^{\frac{1}{n}} \right] + \frac{ETa}{n} \left[\ln \left(\frac{C_o}{C} \right) \right]^{\frac{1-n}{n}} \quad (2)$$

Equation (3) expressed the LDF model⁵⁵.

$$\frac{\partial C}{\partial t} = \frac{F_o D_s}{R_p^2} (C_o - C) \quad (3)$$

where,

$$D_s = D_{so} \exp \left(- \frac{E_a}{RT} \right) \quad (4)$$

Mass balance

Salt and desalinated water;

$$\frac{dM_{sw, \text{evap}}}{dt} = m_{sw, i} - m_{p, \text{cond}} - m_b \quad (5)$$

Salt and evaporator;

$$\frac{dM_{sw, \text{evap}}}{dt} = m_{sw, i} - m_b - \left(\frac{dC_{ads}}{dt} \right) M_{Max} \quad (6)$$

$$M_{sw, \text{eva}} \frac{dX_{sw, \text{eva}}}{dt} = X_{sw, \text{in}} m_{sw, i} - X_{sw, i} m_b - X_D \left(\frac{dC_{ads}}{dt} \right) M_{Max} \quad (7)$$

Energy balance

Evaporator;

$$\begin{aligned} & [M_{s,eva}c_{ps}(T_{eva}, X_{s,eva}) + M_{cu,eva}c_{p,cu,eva}] \frac{dT_{eva}}{dt} \\ & = h_f(T_{eva}, X_{s,eva})m'_{s,i} - h_{fg}(T_{eva}) \frac{dC_{des}}{dt} M_{Max} + m'_{ch}c_{pch}(T_{ch,i} - T_{ch,o}) - h_f(T_{eva}, X_{s,eva}) \end{aligned} \quad (8)$$

Condenser;

$$\begin{aligned} & [(M_{cp})_{cu} + (M_{cp})_{iron} + (M_{cp})_{cw}] \frac{dT_{cond}}{dt} \\ & = h_f(T_{cond}) \frac{dM_d}{dt} + h_{fg}(T_{cond}) \frac{dC_{des}}{dt} M_{Max} + m'_{cw}c_{pcw}(T_{cond})(T_{w,i} - T_{w,o})^{cond} m'_d \end{aligned} \quad (9)$$

Adsorption bed;

$$\begin{aligned} & [(M_{cp})_{iron} + (M_{cp})_{cu} + (M_{cp})_{al} + (M_{cp})_{Max} + M_{Max}C_p] \frac{dT_{bed}}{dt} \\ & = M_{Max}H_{st} \frac{dC_{bed}}{dt} - m'_{w}c_{pw}(T_{w,o} - T_{w,i})^{bed} \end{aligned} \quad (10)$$

The $T_{w,o}$ for each heat exchanger;

$$T_{w,o} = T_{hex} + (T_{w,i} - T_{hex}) \exp\left(\frac{-UA_{hex}}{(m'c_p)_w}\right) \quad (11)$$

The amount of heat in water processes;

$$Q_{des} = \int_0^{t_{cycle}} m'_{hw}c_{pw}(T_{hw,i} - T_{hw,o})dt \quad (12)$$

$$Q_{cond} = \int_0^{t_{cycle}} m'_{cw}c_{pw}(T_{cw,i} - T_{cw,o})dt \quad (13)$$

$$Q_{eva} = \int_0^{t_{cycle}} m'_{ch}c_{pch}(T_{ch,i} - T_{ch,o})dt \quad (14)$$

Performance indicators

$$SDWP = \int_0^{t_{cycle}} \frac{m'_{cw}c_{pw}(T_{cw,o} - T_{cw,i})\tau}{h_{fg}M_{Max}} dt \quad (15)$$

$$SCP = \int_0^{t_{cycle}} \frac{m'_{ch}c_{pch}(T_{ch,i} - T_{ch,o})}{M_{Max}} dt \quad (16)$$

$$COP = \int_0^{t_{cycle}} \frac{m'_{ch}c_{pch}(T_{ch,i} - T_{ch,o})}{m'_{hw}c_{pw}(T_{hw,i} - T_{hw,o})} dt \quad (17)$$

$$GOR = \int_0^{t_{cycle}} \frac{m'_d h_{fg}}{m'_{cw}c_{pw}(T_{cw,i} - T_{cw,o})} dt \quad (18)$$

DATA AVAILABILITY

Raw datasets generated during the current study are available from the corresponding author upon reasonable request.

CODE AVAILABILITY

Code available from the corresponding author upon reasonable request.

Received: 17 May 2022; Accepted: 15 December 2022;

Published online: 11 January 2023

REFERENCES

- Harby, K., Ali, E. S. & Almohammadi, K. M. A novel combined reverse osmosis and hybrid absorption desalination-cooling system to increase overall water recovery and energy efficiency. *J. Clean. Prod.* **287**, 125014 (2021).
- Ghazy, M., Ibrahim, E. M. M., Mohamed, A. S. A. & Askalany, A. A. Cooling technologies for enhancing photovoltaic-thermal (PVT) performance: a state of the art. *Int. J. Energy Environ. Eng.* (2022). <https://doi.org/10.1007/s40095-022-00491-8>.

- Alsaman, A. S. et al. Hybrid solar-driven desalination/cooling systems: Current situation and future trend. *Energies* **15**, 8099 (2022).
- Askalany, A. A. & Ali, E. S. A new approach integration of ejector within adsorption desalination cycle reaching COP higher than one. *Sustain. Energy Technol. Assess.* **41**, 100766 (2020).
- Ali, E. S., Askalany, A. A. & Zohir, A. E. Innovative employing of salt hydration with adsorption to enhance performance of desalination and heat transformation systems. *Appl. Therm. Eng.* **179**, 115614 (2020).
- Ghazy, M., Ibrahim, E. M. M., Mohamed, A. S. A. & Askalany, A. A. Experimental investigation of hybrid photovoltaic solar thermal collector (PV/T)-adsorption desalination system in hot weather conditions. *Energy* **254**, 124370 (2022).
- Alsaman, A. S., Askalany, A. A., Harby, K. & Ahmed, M. S. A state of the art of hybrid adsorption desalination-cooling systems. *Renew. Sustain. Energy Rev.* **58**, 692–703 (2016).
- Mohammed, R. H. et al. Metal-organic frameworks in cooling and water desalination: Synthesis and application. *Renew. Sustain. Energy Rev.* **149**, 111362 (2021).
- Thu, K., Saha, B. B., Chua, K. J. & Ng, K. C. Performance investigation of a waste heat-driven 3-bed 2-evaporator adsorption cycle for cooling and desalination. *Int. J. Heat. Mass Transf.* **101**, 1111–1122 (2016).
- Ali, E. S., Muhammad Asfahan, H., Sultan, M. & Askalany, A. A. A novel ejectors integration with two-stages adsorption desalination: Away to scavenge the ambient energy. *Sustain. Energy Technol. Assess.* **48**, 101658 (2021).
- Mitra, S., Kumar, P., Srinivasan, K. & Dutta, P. Performance evaluation of a two-stage silica gel + water adsorption based cooling-cum-desalination system. *Int. J. Refrig.* **58**, 186–198 (2015).
- Zohir, A. E. et al. A state-of-the-art of experimentally studied adsorption water desalination systems. *Int. J. Energy Environ. Eng.* (2022). <https://doi.org/10.1007/s40095-022-00536-y>.
- Ghazy, M. et al. Solar powered adsorption desalination system employing CPO-27(Ni). *J. Energy Storage* **53**, 105174 (2022).
- Kim, Y. D., Thu, K. & Ng, K. C. Adsorption characteristics of water vapor on ferroaluminophosphate for desalination cycle. *Desalination* **344**, 350–356 (2014).
- Youssef, P. G., Mahmoud, S. M. & AL-Dadah, R. K. Performance analysis of four bed adsorption water desalination/refrigeration system, comparison of AQSOA-202 to silica-gel. *Desalination* **375**, 100–107 (2015).
- Pinheiro, J. M. et al. Application of the novel ETS-10/water pair in cyclic adsorption heating processes: Measurement of equilibrium and kinetics properties and simulation studies. *Appl. Therm. Eng.* **87**, 412–423 (2015).
- Elsayed, E. et al. Development of MIL-101(Cr)/GrO composites for adsorption heat pump applications. *Microporous Mesoporous Mater.* **244**, 180–191 (2017).
- Askalany, A. et al. Experimental optimization of the cycle time and switching time of a metal organic framework adsorption desalination cycle. *Energy Convers. Manag.* **245**, 114558 (2021).
- Alsaman, A. S., Ibrahim, E. M. M., Ahmed, M. S. & Askalany, A. A. Composite adsorbent materials for desalination and cooling applications: A state of the art. *Int. J. Energy Res.* **46**, 10345–10371 (2022).
- Alsaman, A. S. et al. Experimental investigation of sodium polyacrylate-based innovative adsorbent material for higher desalination and cooling effects. *Energy Convers. Manag.* **266**, 115818 (2022).
- Alsaman, A. S. et al. Characterization and cost analysis of a modified silica gel-based adsorption desalination application. *J. Clean. Prod.* **134614** (2022). <https://doi.org/10.1016/j.jclepro.2022.134614>.
- Askalany, A. A. et al. High potential of employing bentonite in adsorption cooling systems driven by low grade heat source temperatures. *Energy* **141**, 782–791 (2017).
- Wahono, S. K. et al. Plasma activation on natural mordenite-clinoptilolite zeolite for water vapor adsorption enhancement. *Appl. Surf. Sci.* **483**, 940–946 (2019).
- Gordeeva, L. G., Glaznev, I. S., Malakhov, V. V. & Aristov, Y. I. Influence of calcium chloride interaction with silica surface on phase composition and sorption properties of dispersed salt. *Russ. J. Phys. Chem.* **77**, 1843–1847 (2003).
- Ponomarenko, I. V., Glaznev, I. S., Gubar, A. V., Aristov, Y. I. & Kirik, S. D. Synthesis and water sorption properties of a new composite 'CaCl2 confined into SBA-15 pores'. *Microporous Mesoporous Mater.* **129**, 243–250 (2010).
- Jabbari-Hichri, A., Bennici, S. & Auroux, A. Effect of aluminum sulfate addition on the thermal storage performance of mesoporous SBA-15 and MCM-41 materials. *Sol. Energy Mater. Sol. Cells* **149**, 232–241 (2016).
- Ristić, A. & Logar, N. Z. New composite water sorbents CaCl2-PHTS for low-temperature sorption heat storage: Determination of structural properties. *Nanomaterials* **9**, 27 (2019).
- Askalany, A. et al. Silica-Supported Ionic Liquids for Heat-Powered Sorption Desalination. *ACS Appl. Mater. Interfaces* **11**, 36497–36505 (2019).
- Alsaman, A. S. et al. Composite material-based a clay for adsorption desalination and cooling applications. *Chem. Eng. Res. Des.* (2022). <https://doi.org/10.1016/j.cherd.2022.09.017>.

30. Ng, K. C., Saha, B. B., Chakraborty, A. & Koyama, S. Adsorption desalination quenches global thirst. *Heat. Transf. Eng.* **29**, 845–848 (2008).
31. Chakraborty, A., Saha, B. B., Koyama, S., Ng, K. C. & Srinivasan, K. Adsorption thermodynamics of silica gel-water systems. *J. Chem. Eng. Data* **54**, 448–452 (2009).
32. Mitra, S., Thu, K., Saha, B. B., Srinivasan, K. & Dutta, P. Modeling study of two-stage, multi-bed air cooled silica gel + water adsorption cooling cum desalination system. *Appl. Therm. Eng.* **114**, 704–712 (2017).
33. Thu, K., Yanagi, H., Saha, B. B. & Ng, K. C. Performance investigation on a 4-bed adsorption desalination cycle with internal heat recovery scheme. *Desalination* **402**, 88–96 (2017).
34. Jozefaciuk 2002. G. D. A.-O. 1. Effect of Acid and Alkali Treatments on Surface-Charge Properties of Selected Minerals. *Clays Clay Miner.* **50**, 647–656 (2002).
35. Belver, C., Bañares Muñoz, M. A. & Vicente, M. A. Chemical activation of a kaolinite under acid and alkaline conditions. *Chem. Mater.* **14**, 2033–2043 (2002).
36. Temuujin, J. et al. Characterisation of acid activated montmorillonite clay from Tuulant (Mongolia). *Ceram. Int.* **30**, 251–255 (2004).
37. Ali, E. S. et al. Experimental adsorption water desalination system utilizing activated clay for low grade heat source applications. *J. Energy Storage* **43**, 103219 (2021).
38. Krupskaya, V. V. et al. Experimental study of montmorillonite structure and transformation of its properties under treatment with inorganic acid solutions. *Minerals* **7**, (2017).
39. Rodrigues Mota, T. L., Marques de Oliveira, A. P., Nunes, E. H. M. & Houmard, M. Simple process for preparing mesoporous sol-gel silica adsorbents with high water adsorption capacities. *Microporous Mesoporous Mater.* **253**, 177–182 (2017).
40. Teo, H. W. B., Chakraborty, A. & Kayal, S. Formic acid modulated (fam) aluminium fumarate MOF for improved isotherms and kinetics with water adsorption: Cooling/heat pump applications. *Microporous Mesoporous Mater.* **272**, 109–116 (2018).
41. Komadel, P. & Madejová, J. Chapter 7.1 Acid Activation of Clay Minerals. *Dev. Clay Sci.* **1**, 263–287 (2006).
42. Mangun, C. L., Daley, M. A., Braatz, R. D. & Economy, J. Effect of pore size on adsorption of hydrocarbons in phenolic-based activated carbon fibers. *Carbon N. Y.* **36**, 123–129 (1998).
43. Askalany, A., Habib, K., Ghazy, M. & Assadi, M. K. Adsorption cooling system employing activated carbon/hfc410a adsorption pair. *ARPN J. Eng. Appl. Sci.* **11**, 12253–12257 (2016).
44. Gordeeva, L. G., Restuccia, G., Freni, A. & Aristov, Y. I. *Water sorption on composites 'LiBr in a porous carbon'*. *Fuel Processing Technology* vol. 79 www.elsevier.com/locate/fuproc (2002).
45. Tso, C. Y. & Chao, C. Y. H. Activated carbon, silica-gel and calcium chloride composite adsorbents for energy efficient solar adsorption cooling and dehumidification systems. *Int. J. Refrig.* **35**, 1626–1638 (2012).
46. Huang, H. et al. Development research on composite adsorbents applied in adsorption heat pump. *Appl. Therm. Eng.* **30**, 1193–1198 (2010).
47. Casey, S. P., Elvins, J., Riffat, S. & Robinson, A. Salt impregnated desiccant matrices for 'open' thermochemical energy storage - Selection, synthesis and characterisation of candidate materials. *Energy Build.* **84**, 412–425 (2014).
48. Yu, Q. et al. Characterization of MgCl₂/AC composite adsorbent and its water vapor adsorption for solar drying system application. *Renew. Energy* **138**, 1087–1095 (2019).
49. Grekova, A., Gordeeva, L. & Aristov, Y. Composite sorbents 'Li/Ca halogenides inside Multi-wall Carbon Nano-tubes' for Thermal Energy Storage. *Sol. Energy Mater. Sol. Cells* **155**, 176–183 (2016).
50. Grekova, A. D., Gordeeva, L. G., Lu, Z., Wang, R. & Aristov, Y. I. Composite "LiCl/MWCNT" as advanced water sorbent for thermal energy storage: Sorption dynamics. *Sol. Energy Mater. Sol. Cells* **176**, 273–279 (2018).
51. Brancato, V. et al. Water adsorption equilibrium and dynamics of LiCl/MWCNT/PVA composite for adsorptive heat storage. *Sol. Energy Mater. Sol. Cells* **193**, 133–140 (2019).
52. Polarz, S. & Smarsly, B. Nanoporous materials. *J. Nanosci. Nanotechnol.* **2**, 581–612 (2002).
53. Mitra, S., Srinivasan, K., Kumar, P., Murthy, S. S. & Dutta, P. Solar driven adsorption desalination system. *Energy Procedia* **49**, 2261–2269 (2014).
54. Ng, K. C., Thu, K., Saha, B. B. & Chakraborty, A. Study on a waste heat-driven adsorption cooling cum desalination cycle. *Int. J. Refrig.* **35**, 685–693 (2012).
55. Alsaman, A. S., Askalany, A. A., Harby, K. & Ahmed, M. S. Performance evaluation of a solar-driven adsorption desalination-cooling system. *Energy* **128**, 196–207 (2017).
56. Ng, K. C., Thu, K., Chakraborty, A., Saha, B. B. & Chun, W. G. Solar-assisted dual-effect adsorption cycle for the production of cooling effect and potable water. *Int. J. Low-Carbon Technol.* **4**, 61–67 (2009).
57. Youssef, P. G., Al-Dadah, R. K., Mahmoud, S. M., Dakkama, H. J. & Elsayed, A. Effect of evaporator and condenser temperatures on the performance of adsorption desalination cooling cycle. *Energy Procedia* **75**, 1464–1469 (2015).
58. Stadie, N. P., Purewal, J. J., Ahn, C. C. & Fultz, B. Measurements of hydrogen spillover in platinum doped superactivated carbon. *Langmuir* **26**, 15481–15485 (2010).
59. Ali, E. S. et al. Novel ultrasonic dynamic vapor sorption apparatus for adsorption drying, cooling and desalination applications. *Energy Rep.* **8**, 8798–8804 (2022).
60. Ali, E. S., Askalany, A. A., Harby, K., Diab, M. R. & Alsaman, A. S. Adsorption desalination-cooling system employing copper sulfate driven by low-grade heat sources. *Appl. Therm. Eng.* **136**, 169–176 (2018).
61. Ghazy, M. et al. Performance enhancement of adsorption cooling cycle by pyrolysis of Maxsorb III activated carbon with ammonium carbonate. *Int. J. Refrig.* **126**, 210–221 (2021).

ACKNOWLEDGEMENTS

This research is supported by Science, Technology & Innovation Funding Authority (STDF) through Call 8/Innovation Grants (STDF-IG)/Development & Innovation Grants. Project No 43579.

AUTHOR CONTRIBUTIONS

A.S.A.: Validation, Investigation, Theoretical modeling, Writing—original draft, Visualization, Writing—review & editing. E.M.M.I.: Supervision, Writing—review & editing. M.S.A.: Supervision, Writing—review & editing. E.S.A.: Validation, Investigation, Theoretical modeling, Writing—original draft, Visualization. A.M.F.: Validation, Investigation, Visualization. A.A.: Conceptualization, Methodology, Supervision, Writing—review & editing.

FUNDING

Open access funding provided by The Science, Technology & Innovation Funding Authority (STDF) in cooperation with The Egyptian Knowledge Bank (EKB).

COMPETING INTERESTS

The authors declare competing interests.

ADDITIONAL INFORMATION

Correspondence and requests for materials should be addressed to Ahmed A. Askalany.

Reprints and permission information is available at <http://www.nature.com/reprints>

Publisher's note Springer Nature remains neutral with regard to jurisdictional claims in published maps and institutional affiliations.



Open Access This article is licensed under a Creative Commons Attribution 4.0 International License, which permits use, sharing, adaptation, distribution and reproduction in any medium or format, as long as you give appropriate credit to the original author(s) and the source, provide a link to the Creative Commons license, and indicate if changes were made. The images or other third party material in this article are included in the article's Creative Commons license, unless indicated otherwise in a credit line to the material. If material is not included in the article's Creative Commons license and your intended use is not permitted by statutory regulation or exceeds the permitted use, you will need to obtain permission directly from the copyright holder. To view a copy of this license, visit <http://creativecommons.org/licenses/by/4.0/>.

© The Author(s) 2023